Realization of a highly sensitive mass sensor in a quadratically coupled optomechanical system

Shaopeng Liu, Bo Liu,* Junfeng Wang, and Tingting Sun
School of Physics and Optoelectronic Engineering, Nanjing University of Information Science and Technology, Nanjing 210044, China

Wen-Xing Yang
School of Physics, Southeast University, Nanjing 211189, China

(Received 28 July 2018; published 11 March 2019)

We propose and analyze an efficient scheme for realizing high-sensitive mass sensor in a quadratically coupled optomechanical system via nonlinear second-order sideband process. This is achieved by exploiting a well-established optomechanical circumstance, where a degenerate parametric amplifier (DPA) is embedded into a membrane-in-the-middle cavity driven by a strong control field and a weak probe pulse. Beyond the conventional linearized approximation, we derive analytical expressions for the efficiency of a second-order sideband and the sensitivity of a mass sensor by using a perturbation method. In this scheme, an added mass deposited on the dielectric membrane can be measured by monitoring the efficiency variation of second-order sideband generation. Using experimentally achievable parameters, we identify the conditions under which nonlinear gain of DPA allows us to enhance the efficiency of a second-order sideband and improve the sensitivity of a mass sensor beyond what is achievable in the linearly coupled optomechanical system based on the detection of mechanical frequency shift. More importantly, we also find that the maximum efficiency of a second-order sideband and the optimum sensitivity of a mass sensor simultaneously serve as an efficient detection for the added mass of a membrane when a control field and nonlinear gain of DPA become strong. The present proposal offers a practical opportunity to design an all-optical nonlinear mass sensor at the picogram level.

DOI: 10.1103/PhysRevA.99.033822

I. INTRODUCTION

Cavity optomechanics [1], arming to combine an optical degree of freedom with mechanical degree of freedom via a radiation-pressure force, has been an active disciplinary field for exploring the boundary between quantum and classical physics. It is known that, based on the feedback-backaction of radiation-pressure force, the effective frequency of optical cavity $\omega(x) = \omega_c + \omega_f(x)$ in all optomechanical systems is characterized by a superposition of the intrinsic cavity frequency ω_c and the frequency shift of cavity $\omega_f(x) = \frac{\partial\omega}{\partial x}x + \frac{1}{2}\frac{\partial^2\omega}{\partial x^2}x^2$, in which $\omega_f(x)$ originates from the linear and quadratic optomechanical coupling between optical and mechanical degrees of freedom [2]. In the linear optomechanical coupling regime, the effective frequency of a cavity is approximatively proportional to the displacement of a mechanical mode: $\omega(x) \propto x$. It enables a direct measurement for the displacement of a mechanical mode [3]. Particularly, as the linear optomechanical coupling reaches a radiation-pressure strong-coupling regime, a variety of optical phenomena have been theoretically and experimentally discovered, such as optomechanically induced transparency (OMIT) [4,5], sideband cooling of mechanical resonator [6–8], higher-order sideband generation [9–15], and the production of squeezed states [16–21].

Recently, an optomechanical device featuring pure quadratic optomechanical coupling has been fabricated in the high-finesse Fabry-Pérot cavity [22–24], where a flexible dielectric membrane is accurately positioned at a node or antinode of the intracavity standing wave. One advantage of this quadratically coupled optomechanical system is the quantum nondemolition readout of a membrane energy eigenstate [22,23,25], which arises from a linear relation between the position-dependent cavity frequency and the square displacement of the membrane, i.e., $\omega(x) \propto x^2$. This quadratic optomechanical coupling has been used to induce unique optical phenomena including two-phonon OMIT [26,27] and amplification [24,28,29], quantum phase transition [30], and the preparation of squeezed states and superposition states [31–34].

On the other hand, the special structure of cavity optomechanics, which consists of the high-Q optical cavity and the small mass of a mechanical object, has provided an excellent platform for studying manipulation of output light and developing high-precision measurement for electrical charge, mass, and weak force [35–50]. Note that all of these precision measurements in optomechanical system are designed by seeking the correlations between output spectra and measured physical quantities. For example, several groups [35–38] presented the electrical charge detection in a linear optomechanical system, where the mechanical oscillator is coupled to an adjoining charged body via Coulomb interaction. Then one found that the probe transmission or sideband spectrum depends crucially on the electrical charges, which leads to a correlation between the electrical charges and the output spectrum. Other schemes [39–43] about all-optical mass sensors were also proposed by establishing a direct relationship

*bo@nuist.edu.cn

between the mass change of a mechanical resonator and the frequency shift of the output spectrum in a linear optomechanical microresonator. More interestingly, in comparison with precision measurement in an electrical device, all-optical measurement in an optomechanical device has ultralow heat loss, broadband frequency of the detection region, and higher accuracy.

It is worth noting that the detection capability of an optomechanical device is always governed by few noise processes that cause the fluctuation of the output spectrum and the uncertainty while detecting targets. Two main noise sources of cavity optomechanics are extrinsic and intrinsic noises [51]. Although it is very difficult to avoid these noise processes in precision measurement, there are several effective methods for reducing the noise levels. First, extrinsic noise in the form of detection noise can be suppressed by making use of a nonlinear parametrically driven sensor and other sophisticated readout equipments [45–47,52]. Second, the composition of intrinsic noise mostly includes mechanical thermal noise, Brownian motion of mechanical elements, and photon shot noise. By employing the advanced techniques of sideband cooling and squeezed light in an optomechanical system, these intrinsic noises can be reduced to a low-noise level, even to below the standard quantum limit [6–8,20,21,31,49]. Based on these technical achievements, it reminds us of one question: Could high-precision measurement for the added mass and the eigenenergy of a membrane be achieved in the quadratically coupled optomechanical system?

In this paper, we demonstrate that a quadratically coupled optomechanical system assisted by DPA is suggested to realize the all-optical nonlinear mass sensor. This scheme involving a nonlinear second-order sideband is dependent upon an observable correlation between the added mass of a mechanical object and the efficiency variation of an output sideband spectrum. Using experimentally achievable parameters, our results illustrate that the nonlinear gain of DPA allows us to enhance the efficiency of a generated second-order sideband and improve the sensitivity of nonlinear mass measurement. In the presence of a strong control field and DPA, it is found that the maximum efficiency of a second-order sideband and the corresponding optimum sensitivity simultaneously serve as an efficient monitor for the added mass and the eigenenergy of membrane. From the viewpoint of application, the present optomechanical system is suitable for establishing an all-optical mass sensor at the picogram (pg) level.

In comparison with previous work [29], we emphasize that, differently from the mechanism of two-phonon sideband amplification induced by an external mechanical pump in Ref. [29], the enhanced second-order sideband in the present scheme is achieved as a result of DPA-induced nonlinear parametrical process. With the help of a nonlinear parametrical process, we analyze that DPA-induced noise squeezing and cooling have a robust ability for resisting various noises in the process of mass detection. But the previous work in Ref. [29] aims only at amplifying a nonlinear sideband spectrum by employing an external mechanical pump. This external mechanical pump carries an amount of mechanical thermal noise, which is unsuitable for the precision measurement of ultrasmall mass.

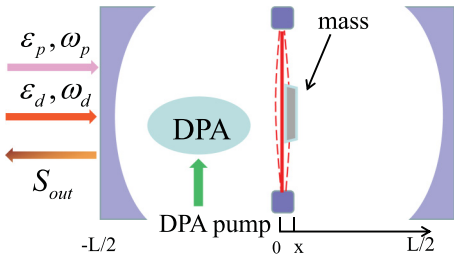

FIG. 1. Schematic diagram of a quadratically coupled optomechanical system. A DPA is embedded in the optomechanical cavity, while a thin dielectric membrane is located at an antinode of the cavity field. This quadratically coupled optomechanical system is driven by a strong control field (with frequency ω_d) and a relatively weak probe pulse (with frequency ω_p).

II. THEORETICAL MODEL AND BASIC EQUATIONS IN THE QUADRATICALLY COUPLED OPTOMECHANICAL SYSTEM

As schematically shown in Fig. 1, a quadratically coupled optomechanical setup is made up of two fixed high-finesse mirrors separated from each other by a distance L and a thin dielectric membrane with angular frequency ω_m, effective mass m_m, and finite reflectivity R. The DPA embedded in the optomechanical cavity is expected for amplifying nonlinear optical responses of system and reducing mechanical thermal noise and photon shot noise. As verified in Refs. [20,49,53], the operating mechanism of DPA is standard two-photon squeezing. The optomechanical system assisted by DPA provides an excellent circumstance, where the squeezed state transfers between a photon of a cavity field and a phonon of mechanical mode. When this quadratically coupled optomechanical system is driven by the input field $S_{in} = \varepsilon_d e^{-i\omega_d t} + \varepsilon_p e^{-i\omega_p t}$ ($\varepsilon_{d,p}$ and $\omega_{d,p}$ denote the amplitudes and center frequencies of the continuous-wave control field and probe pulse, respectively), a radiation-pressure force acts on the movable membrane and triggers the generation of quadratic optomechanical coupling by ensuring that the membrane is located at an antinode of the intracavity field. Then the effective frequency of the cavity is approximated to the second-order term of displacement: $\omega(x) = \omega_c + \frac{1}{2}\frac{\partial^2\omega}{\partial x^2}x^2$. The quadratic optomechanical coupling constant is defined as $G = \frac{1}{2}\frac{d^2\omega}{dx^2}|_{x=0} = \frac{8\pi^2 c}{L\lambda_d^2}\sqrt{\frac{R}{1-R}}$ [2,26] with the speed of light c in vacuum and the wavelength of control field λ_d.

In a rotating frame at the frequency of control field ω_d, we begin our analysis by writing the interaction Hamiltonian of the quadratically coupled optomechanical system:

$$\begin{aligned}\hat{H}_{\rm int} = {} & \frac{\hat{p}^2}{2m} + \frac{1}{2}m\omega_m^2\hat{x}^2 + \hbar\Delta_c\hat{a}^\dagger\hat{a} + i\hbar\sqrt{\eta_L\kappa}\varepsilon_d(\hat{a}^\dagger - \hat{a}) \\ & + \hbar G\hat{a}^\dagger\hat{a}\hat{x}^2 + i\hbar\sqrt{\eta_L\kappa}\varepsilon_p(\hat{a}^\dagger e^{-i\Delta_p t} - \hat{a}e^{i\Delta_p t}) \\ & + i\hbar G_a(\hat{a}^{\dagger 2}e^{-i\Delta_p t}e^{i\theta} - \hat{a}^2 e^{i\Delta_p t}e^{-i\theta}). \end{aligned} \quad (1)$$

The first two terms in the above Hamiltonian represent the energy of a membrane, where $\hat{x}$ and $\hat{p}$ are the position and the momentum operators of a membrane, respectively. $\hat{a}$ ($\hat{a}^\dagger$) denotes the bosonic annihilation (creation) operator of the cavity mode. The corresponding frequency detunings are

defined as $\Delta_c = \omega_c - \omega_d$ and $\Delta_p = \omega_p - \omega_d$. In the DPA, we assume that this DPA with a second-order nonlinearity crystal is excited by a pump driving with the frequency $\omega_p + \omega_d$ and the phase θ, so that the signal light and the idler light in DPA have the same frequency $\frac{1}{2}(\omega_p + \omega_d)$. G_a is the nonlinear gain of DPA, which can be controlled and adjusted by the pump driving [54,55]. The total mass of membrane $m = m_m + \delta_m$ includes the intrinsic membrane mass m_m and the added mass δ_m. Usually, this added mass deposited onto the surface of a membrane modifies the nonlinear dynamics of a membrane and the interaction between optical and mechanical degrees of freedom and ultimately results in an obvious variation in linear and nonlinear output spectra. In addition, the amplitudes $\varepsilon_{d,p}$ of the control field and probe pulse can be normalized to a photon flux at the input of the cavity [4], $\varepsilon_{d,p} = \sqrt{P_{d,p}/\hbar\omega_{d,p}}$, with control field and probe pulse powers $P_{d,p}$. The total loss rate is described as $\kappa = \kappa_0 + \kappa_L + \kappa_R$ with an intrinsic loss rate κ_0 and an external loss rate of left (right) mirror $\kappa_L = \eta_L\kappa$ ($\kappa_R = \eta_R\kappa$), where the coupling parameter $\eta_{L,R}$ can be continuously adjusted [56].

It is well known that, taking the cavity damping and the dissipation process into consideration, the motion dynamics for all of the optomechanical system can be fully described by the Heisenberg-Langevin equations. After employing some shorthand definitions for the Heisenberg operators, $\hat{X} = \hat{x}^2$, $\hat{P} = \hat{p}^2$, and $\hat{Q} = \hat{x}\hat{p} + \hat{p}\hat{x}$, one readily obtains the following Heisenberg-Langevin equations:

$$\partial_t\hat{a} = -\left[\frac{\kappa}{2} + i(\Delta_c + G\hat{X})\right]\hat{a} + 2G_a\hat{a}^\dagger e^{-i\Delta_p t}e^{i\theta} + \sqrt{\eta_L\kappa}(\varepsilon_c + \varepsilon_p e^{-i\Delta_p t}) + \sqrt{\eta_L\kappa}\hat{a}_{in}, \tag{2}$$

$$\partial_t\hat{x} = \frac{\hat{p}}{m}, \tag{3}$$

$$\partial_t\hat{p} = -m\omega_m^2\hat{x} - \Gamma_m\hat{p} - 2\hbar G\hat{a}^\dagger\hat{a}\hat{x} + \hat{F}_{th}, \tag{4}$$

$$\partial_t\hat{X} = \frac{\hat{Q}}{m}, \tag{5}$$

$$\partial_t\hat{P} = -\left(2\hbar G\hat{a}^\dagger\hat{a} + m\omega_m^2\right)\hat{Q} - 2\Gamma_m\hat{P} + \hat{F}'_{th}, \tag{6}$$

$$\partial_t\hat{Q} = -\left(4\hbar G\hat{a}^\dagger\hat{a} + 2m\omega_m^2\right)\hat{X} - \Gamma_m\hat{Q} + \frac{2\hat{P}}{m}, \tag{7}$$

where the decay rate κ of the cavity field and the damping Γ_m of the mechanical mode are phenomenologically added in above equations. $\hat{a}_{in}$ is the input vacuum noise operator, while $\hat{F}_{th}$ represents the thermal bath operator of mechanical mode. The expectation values of the two noise operators are zero: $\langle\hat{a}_{in}(t)\rangle = 0$ and $\langle\hat{F}_{th}(t)\rangle = 0$. Their correlation functions are governed by $\langle\hat{a}_{in}(t)\hat{a}^\dagger_{in}(t')\rangle = \delta(t-t')$ and $\langle\hat{F}_{th}(t)\hat{F}_{th}(t')\rangle = \frac{\hbar\Gamma_m m}{2\pi}\int\omega e^{-i\omega(t-t')}[1 + \coth(\frac{\hbar\omega}{2k_BT})]\,d\omega$ with the Boltzmann constant k_B [57]. Note that $\hat{F}'_{th}$ in Eq. (6) represents the derivation of the thermal mechanical operator $\hat{F}_{th}$ and has the form $\hat{F}'_{th} = \hat{p}\hat{F}_{th} + \hat{F}_{th}\hat{p}$. Its expectation value is $\langle\hat{F}'_{th}(t)\rangle = \Gamma_m(1 + 2n_{th})\hbar m\omega_m$, in which $n_{th} = [\exp(\hbar\omega_m/k_BT) - 1]^{-1}$ is the mean thermal phonon number at the thermal equilibrium between the membrane and the thermal environment with temperature T (see the Appendix). For simplicity, we don't consider the phase-dependence effect of DPA and assume $\theta = 0$.

According to the perturbation method used in Ref. [29], the expectation values of the operators in Eqs. (2)–(7) can be expressed as the perturbation forms of $a(t) = a_0 + \sum_n (A_n^- e^{-ni\Delta_p t} + A_n^+ e^{ni\Delta_p t})$ and $\mathcal{O}(t) = \mathcal{O}_0 + \sum_n (\mathcal{O}_n e^{-ni\Delta_p t} + \mathcal{O}_n^* e^{ni\Delta_p t})$ ($\mathcal{O} = X, P, Q$), in which A_n^- (A_n^+) is the amplitude of n-order upper (lower) sideband with the integer n being the order of sideband. By taking these perturbation forms into Eqs. (2)–(7) and comparing the coefficients of the same order, the steady-state solutions of Eqs. (2)–(7) can be obtained as $[a_0, X_0, P_0, Q_0] = [\frac{\sqrt{\eta_L\kappa}\varepsilon_c}{\frac{\kappa}{2} + i\bar{\Delta}_c}, \frac{P_0}{m^2\omega_m^2(1+2\alpha)}, (1 + 2n_{th})\frac{\hbar m\omega_m}{2}, 0]$ with $\bar{\Delta}_c = \Delta_c + GX_0$ and $\alpha = \frac{\hbar G|a_0|^2}{m\omega_m^2}$, while the amplitudes of the first-order sideband and second-order upper sideband are given as

$$A_1^- = \frac{i|a_0|^2\beta_1(\Delta_p) + \beta_2(\Delta_p)}{D(\Delta_p)}(\sqrt{\eta_L\kappa}\varepsilon_p + 2a_0^*G_a), \tag{8}$$

$$A_1^+ = \frac{ia_0^2\beta_1^*(\Delta_p)}{D^*(\Delta_p)}(\sqrt{\eta_L\kappa}\varepsilon_p + 2a_0G_a), \tag{9}$$

$$\begin{aligned} A_2^- = \frac{1}{D(2\Delta_p)}\{&2G_a(A_1^+)^*[\beta_2(2\Delta_p) + i|a_0|^2\beta_1(2\Delta_p)] \\ &+ \beta_3(2\Delta_p)(A_1^+)^*X_1 + \beta_4(2\Delta_p)A_1^-X_1 \\ &+ ia_0f_2(2\Delta_p)\beta_1(2\Delta_p)(A_1^+)^*A_1^-\}, \end{aligned} \tag{10}$$

with

$$\begin{aligned} f_1(n\Delta_p) &= \frac{\kappa}{2} + i\bar{\Delta}_c - in\Delta_p, \\ f_2(n\Delta_p) &= \frac{\kappa}{2} - i\bar{\Delta}_c - in\Delta_p, \\ f_3(n\Delta_p) &= 2\Gamma_m - in\Delta_p, \\ f_4(n\Delta_p) &= (4\alpha + 2)\omega_m^2 - in\Delta_p(\Gamma_m - in\Delta_p), \\ \beta_1(n\Delta_p) &= 4G^2\hbar X_0\frac{f_3(n\Delta_p)}{mf_2(n\Delta_p)}, \\ \beta_2(n\Delta_p) &= f_3(n\Delta_p)f_4(n\Delta_p) - i(4\alpha + 2)n\Delta_p\omega_m^2, \\ \beta_3(n\Delta_p) &= 4\Delta_p\hbar G^2a_0^2/m + 4i\hbar G^2a_0^2f_3(n\Delta_p)/m \\ &\quad - Ga_0^2\beta_1(n\Delta_p), \\ \beta_4(n\Delta_p) &= 4\Delta_p\hbar G^2|a_0|^2/m + 4i\hbar G^2|a_0|^2f_3(n\Delta_p)/m \\ &\quad + G|a_0|^2\beta_1(n\Delta_p) - iG\beta_2(n\Delta_p), \\ D(n\Delta_p) &= -2\bar{\Delta}|a_0|^2\beta_1(n\Delta_p) + f_1(n\Delta_p)\beta_2(n\Delta_p), \\ X_1 &= \frac{-a_0^*f_2(\Delta_p)\beta_1(\Delta_p)}{GD(\Delta_p)}(\sqrt{\eta_L\kappa}\varepsilon_p + 2a_0^*G_a). \end{aligned}$$

Subsequently, we concentrate on the output fields that transmit through the left mirror of the cavity. According to the input-output relation of the cavity, we have the output transmission spectrum as

$$\begin{aligned} S_{\text{out}} = \sqrt{\eta_L\kappa}a - S_{in}^I &= c_1 + c_pe^{-i\Delta_p t} + \sqrt{\eta_L\kappa}A_1^+e^{i\Delta_p t} \\ &+ \sqrt{\eta_L\kappa}\sum_{z=2}^{n}(A_z^-e^{-zi\Delta_p t} + A_z^+e^{zi\Delta_p t}), \end{aligned} \tag{11}$$

with $c_1 = \sqrt{\eta_c\kappa}a_0 - \varepsilon_c$ and $c_p = \sqrt{\eta_c\kappa}A_1^- - \varepsilon_p$. S_{in}^I is the transformation form of S_{in} in a rotating frame of control field

frequency. We introduce the dimensionless quantity [9,58]

$$\eta_2 = \left| \frac{\sqrt{\eta_c \kappa} A_2^-}{\varepsilon_p} \right|, \tag{12}$$

which refers to the efficiency of the second-order upper sideband, in which the amplitude of the probe pulse is treated as a basic scale to gauge the amplitude of the output sideband η_2.

Now, we turn to study the realization of a highly sensitive mass sensor. Although the mechanical object of an optomechanical system has minuscule mass (about 10^{-11}–10^{-20} kg), it has a significant influence on optical feedback cooling, transmission spectrum, and sideband spectrum [1–5,9–13]. It may provide the possibility to measure the added mass deposited on the surface of a mechanical object by monitoring the efficiency variation of a second-order sideband. There are two reasons why the second-order sideband is chosen as the detection signal in nonlinear mass sensor: (1) Comparing with linearly mass detection techniques, the mass sensor operating in a nonlinear parametrical region has a great performance on enhancing a nonlinear output signal without amplifying input thermomechanical noise, which is favorable for improving the signal-to-noise ratio [47]. (2) In the nonlinear output spectra, the intensity of a second-order sideband is always stronger than the other higher order sideband signals, which is beneficial for the observation of output signal in an experiment.

In order to evaluate the influence of the added mass on second-order upper sideband η_2, a similar definition used in Ref. [40] for the sensitivity of mass sensor is

$$S = \left| \frac{d\eta_2}{d\delta_m} \right|. \tag{13}$$

The sensitivity indicates the spectrum slope of a second-order sideband with respect to the mass change. More specifically, this sensitivity exhibits the identification ability for the mass change of a membrane in a mass detection process. When a tiny mass deposited on the membrane is measured, the higher the detection sensitivity is, the more obvious the change of an output second-order sideband signal is. It should be noted that the sensitivity mentioned above merely depends on the efficiency variation of second-order sideband efficiency without considering system noise processes. How to exclude the disturbance of system noise processes in a mass sensor will be introduced in Sec. IV.

Based on the above theoretical derivation of the efficiency of a second-order upper sideband and the detection sensitivity, the detailed measurement process in a mass sensor can be illustrated as follows: (1) after the added mass is deposited on the dielectric membrane, a cavity optomechanical system is driven by the strong control field with fixed frequency detuning $\Delta_c = 2\omega_m$, while DPA is driven by a weak pump driving; (2) we apply another probe pulse to scan across the optomechanical cavity, then detect the nonlinear transmission spectrum. By using a similar heterodyne detection scheme as in Ref. [59], the intensity of the second-order sideband can be easily obtained.

It should be emphasized that the currently outstanding technique allows us to integrate a flexible micromechanical object into a high-finesse cavity without compromising the mechanical and optical properties. Experimentally, the quadratically coupled optomechanical system has been reported in the recent Ref. [22], in which the membrane is movable with angular frequency $\omega_m = 2\pi \times 0.1$ MHz, mass $m_m = 100$ pg, reflectivity $R = 0.45$, and mechanical quality factor $Q = \omega_m/\Gamma_m = \pi \times 10^4$. The cavity length L and total loss rate of cavity field κ are estimated to be 67 mm and $0.2\omega_m$, respectively. In this scenario, we assume the wave length of control field $\lambda_d = 2\pi c/\omega_d = 532$ nm and the cavity mode detuning $\Delta_c = 2\omega_m$ for building a two-phonon resonance case in the quadratic optomechanical coupling circumstance.

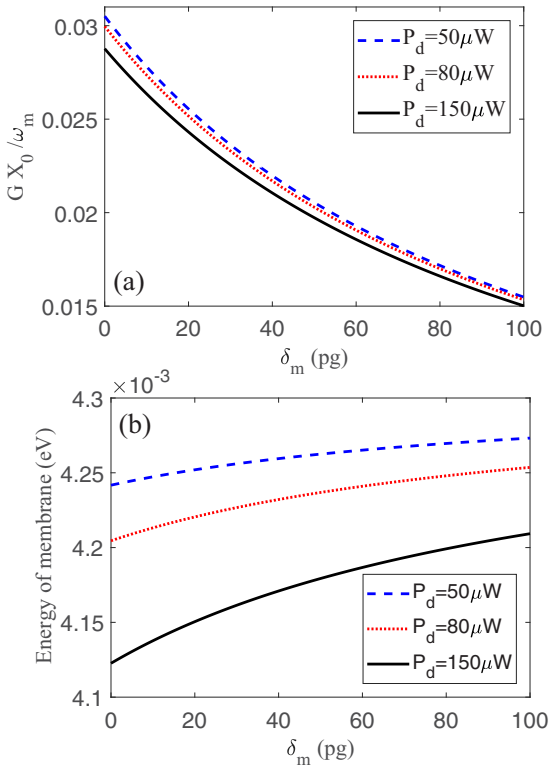

FIG. 2. (a) The steady-state solution of GX_0 and (b) the eigenenergy of a membrane versus the added mass δ_m for different control field intensities $P_d = 50\ \mu$W, 80 μW, and 150 μW. Other parameters are $m_m = 100$ pg, $\omega_m = 2\pi \times 0.1$ MHz, $Q = \omega_m/\Gamma_m = \pi \times 10^4$, $L = 67$ mm, $T = 50$ K, $\kappa = 0.2\omega_m$, $\Delta_c = 2\omega_m$, $\eta_L = 0.499$, and $\varepsilon_p = 0.05\varepsilon_c$, respectively.

III. NUMERICAL RESULTS AND DISCUSSIONS

Within the above practical parameter set, first we analyze the influence of the load mass of a membrane on the steady-state solution of system. Therefore, Fig. 2 shows the steady-state solution of GX_0 and the eigenenergy of membrane $\frac{P_0}{2m} + \frac{1}{2}m\omega_m^2 X_0$ versus the added mass δ_m for three different control field intensities $P_d = 50\ \mu$W, 80 μW, and 150 μW. Associating Fig. 2(a) with Fig. 2(b), one can find that, as the added mass δ_m increases, the steady-state solution of GX_0 in Fig. 2(a) decreases monotonically, while the eigenenergy of the membrane in Fig. 2(b) increases monotonically. Accordingly, the added mass change in the quadratically coupled optomechanical system has a prominent influence on the steady-state solution of the system and the eigenenergy

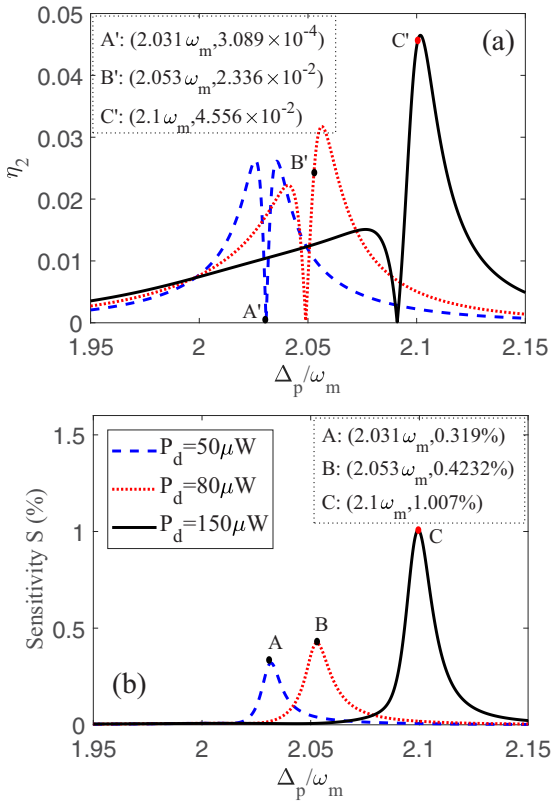

FIG. 3. (a) The efficiency η_2 of a second-order upper sideband and (b) the sensitivity S (in units of pg) of a mass sensor as a function of the probe-pulsed detuning Δ_p for different control field intensities $P_d = 50\ \mu$W (blue dashed line), 80 μW (red dotted line), and 150 μW (black solid line). Other parameters are the same as in Fig. 2 except for $\delta_m = 0$ pg and $G_a = 0$.

of the membrane. From Fig. 2(b), it also shows that, for a fixed added mass, the lowest eigenenergy of membrane occurs in the case of the maximum control field driving with $P_d = 150\ \mu$W. The above interesting result comes from the sideband cooling effect. When the red detuning control field becomes strong, the sideband cooling process of a membrane increases spontaneously [31], causing this decrease of the total energy of membrane. It is worth noting that, based on the premise of mass detection, it may provide a possibility to measure the eigenenergy of a membrane by the functional relationship between the added mass and eigenenergy of a membrane in Fig. 2(b). Now we start to seek the optimized correlation between the output second-order sideband and the added mass deposited on the dielectric membrane. In Fig. 3 we show that the efficiency η_2 of a second-order upper sideband and the sensitivity S of a mass sensor vary with the probe-pulsed detuning Δ_p without the participation of DPA: $G_a = 0$. From the three spectrum lines of Fig. 3 with different control field intensities ($P_d = 50\ \mu$W, 80 μW, and 150 μW), one can find that two located peaks of second-order sideband spectra in Fig. 3(a) appear on both sides of a low-efficiency valley. Correspondingly, the sensitivity S exhibits one located maximum [see points A, B, and C labeled in Fig. 3(b)]. As the control field intensity increases from 50 μW to 80 μW and then to 150 μW, the maximums of both the efficiency η_2 and the sensitivity S have an obvious enhancement, and the positions of these maximums shift toward blue detuning of the probe pulse. In detail, in the case of $P_d = 50\ \mu$W in the blue dashed spectra of Figs. 3(a) and 3(b), the maximum sensitivity S is located at point A ($2.031\omega_m$, 0.319%), while the corresponding efficiency η_2 is located at the low-efficiency valley, point A′ ($2.031\omega_m$, 3.089×10^{-4}). For the case of $P_d = 80\ \mu$W in the red dotted spectra of Figs. 3(a) and 3(b), the maximum sensitivity S is located at point B ($2.053\omega_m$, 0.4232%), while the corresponding efficiency η_2 becomes point B′ ($2.053\omega_m$, 2.336×10^{-2}). If the intensity of the control field reaches 150 μW in the black solid spectra of Figs. 3(a) and 3(b), the maximum sensitivity S is point C ($2.1\omega_m$, 1.007%), while the corresponding efficiency η_2 is near the peak position at point C′ ($2.1\omega_m$, 4.556×10^{-2}). Obviously, both the sensitivity and the corresponding efficiency of a second-order sideband can be simultaneously maximized by employing a strong control driving, $P_d = 150\ \mu$W, which is favorable for designing the high-sensitive mass sensor.

We know that DPA in an optomechanical system has versatile performance for the manipulation of output spectrum [54] and the strong squeezing and sideband cooling of a mechanical mode [20,55]. To explore the role of DPA in this mass sensor, we illustrate the efficiency η_2 of a second-order upper sideband and the sensitivity S of a mass sensor versus the probe-pulsed detuning Δ_p with different nonlinear gain G_a in Figs. 4(a) and 4(b). There are two main characteristics for the efficiency η_2 and the sensitivity S. First, when the nonlinear gain G_a of DPA increases from 0.1κ to 0.6κ, both the efficiency η_2 in Fig. 4(a) and the sensitivity S in Fig. 4(b) can be significantly enhanced. Second, whatever nonlinear gain G_a is to increase, the located maximums of the efficiency η_2 and the sensitivity S are still located at the same position of the probe-pulsed detuning, and the same as that in the black solid spectrum of Fig. 3. This phenomenon can be explained by perturbation theory. Similar to the steady-state solution, the positions of these located maximums or peaks of sideband spectra depend merely on the intrinsic structural parameters of an optomechanical system and the intensity of the control field, rather than the other perturbation terms including probe pulse and nonlinear gain of DPA. As a result, the DPA not only improves the sideband efficiency of a second-order sideband and the sensitivity of a mass sensor, but also keeps the locality of maximum values of the sideband efficiency and the sensitivity.

In order to give a better insight into the effect of DPA on the second-order upper sideband, the efficiency η_2 of a second-order upper sideband and the sensitivity S of a mass sensor versus nonlinear gain G_a of DPA for different probe-pulsed detunings Δ_p are depicted in Fig. 5. The results clearly verify that both the efficiency η_2 in Fig. 5(a) and the sensitivity S in Fig. 5(b) increase monotonically with nonlinear gain G_a increasing. Especially, when nonlinear gain G_a increases from 0 to 0.6κ in the case of $\Delta_p = 2.1\omega_m$ [see the red dotted line in Figs. 5(a) and 5(b)], the quadratically coupled optomechanical system provides an enhancement of more than six times for both the sideband efficiency η_2 and its sensitivity S. Physically, when the DPA is pumped at twice the frequency of the anti-Stokes field, $\frac{1}{2}(\omega_p + \omega_d)$, the parametric frequency conversion between this anti-Stokes field and phonon mode of membrane can provide another way

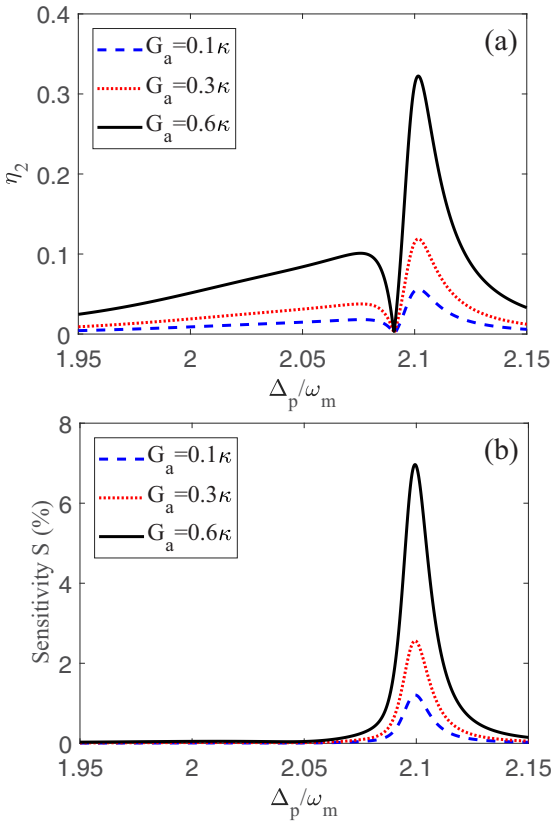

FIG. 4. (a) The efficiency η_2 of a second-order upper sideband and (b) the sensitivity S (in units of pg) of a mass sensor as a function of the probe-pulsed detuning Δ_p for the different nonlinear gain G_a of DPA. Other parameters are the same as in Fig. 2 except for $\delta_m = 0$ pg and $P_d = 150$ μW.

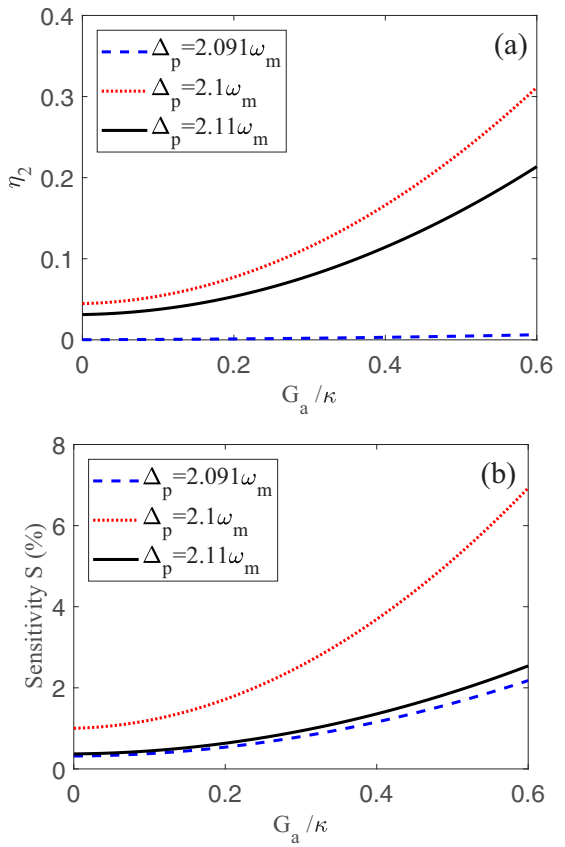

FIG. 5. (a) The efficiency η_2 of a second-order upper sideband and (b) the sensitivity S (in units of pg) of a mass sensor as a function of the nonlinear gain G_a of DPA for different probe-pulsed detunings Δ_p. Other parameters are the same as in Fig. 2 except for $\delta_m = 0$ pg and $P_d = 150$ μW.

to generate an optical second-order sideband, leading to the enhancement of a second-order sideband.

Up to now, we have identified that the efficiency η_2 of a second-order upper sideband and the sensitivity S of a mass sensor can be simultaneously optimized by choosing a strong control driving $P_d = 150$ μW and a strong excitation of DPA with nonlinear gain $G_a = 0.6\kappa$. Based on such an optimized parameter set, a natural question is whether or not this nonlinear mass measurement method is applied to an arbitrary mass deposited on the dielectric membrane, To make an intuitional picture that illustrates the functionality of our proposed mass sensor, we plot the efficiency η_2 of a second-order upper sideband and the sensitivity S of a mass sensor varying with the probe-pulsed detuning Δ_p and the added mass δ_m, as shown in Fig. 6. Associating the efficiency η_2 in Fig. 6(a) with the sensitivity S in Fig. 6(b), it is readily seen that the evolution tendency of maximum efficiency η_2 is consistent with the maximum sensitivity S. Moreover, as the added mass δ_m decreases, both the maximum efficiency η_2 and the corresponding maximum sensitivity S have a remarkable enhancement. In other words, the smaller the added mass is, the more sensitive the detection for a nonlinear second-order sideband spectrum is.

In Fig. 7 we also plot the efficiency η_2 of a second-order upper sideband and the sensitivity S of a mass sensor versus the probe-pulsed detuning Δ_p for different added mass δ_m. Although, as illustrated in Figs. 3–5, the efficiency η_2 and the sensitivity S can be enhanced in the optimized parametric regime, there is a certain extent of mismatching between the maximum efficiency η_2 and the maximum sensitivity S. More specifically, the sensitivities S labeled by points A, B, and C in Fig. 7(b) corresponding to the maximum efficiencies η_2 marked by points A′, B′, and C′ in Fig. 7(a) deviate slightly from the maximum sensitivities (or the peak values) of Fig. 7(b). In analogy with Fig. 3, the located maximum efficiency η_2 and the corresponding sensitivity S in Fig. 7 exhibit an obvious frequency shift when the added mass changes. The physical interpretation is that, according to the perturbation theory, the peak position of sideband spectrum relies sensitively on the intensity of control field and the intrinsic structural parameters of optomechanical system including the mass of membrane.

For our proposed nonlinear mass sensor in the quadratically optomechanical coupled system, the detection sensitivity is an important index for the measurement of a nonlinear second-order sideband spectrum. Due to the existence of mismatching between the maximum efficiency and the maximum sensitivity in the same second-order sideband spectrum as introduced in Fig. 7, we need to define the optimum sensitivity of a mass sensor as $S_{\rm opt}$ that corresponds directly to the maximum efficiency $\eta_2^{\rm max}$ of a second-order upper sideband. By

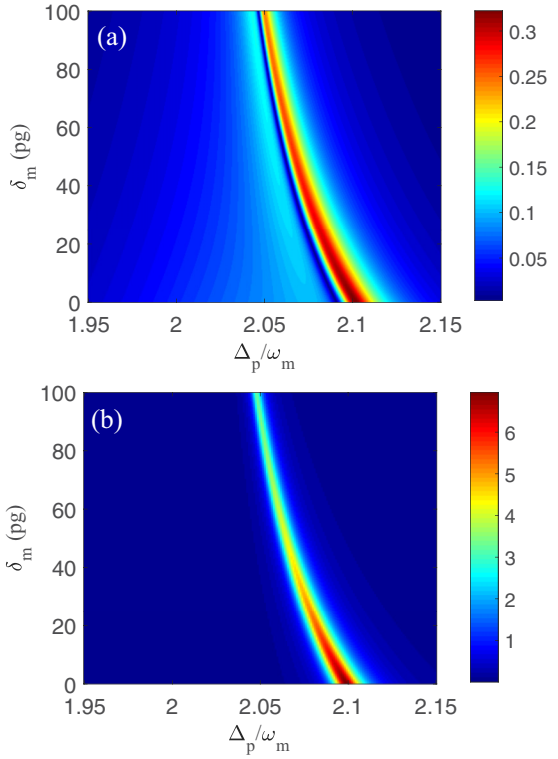

FIG. 6. Contour maps of (a) the efficiency η_2 of a second-order upper sideband and (b) the sensitivity S (in units of pg) of a mass sensor as a function of the probe-pulsed detuning Δ_p and the added mass δ_m. Other parameters are the same as in Fig. 2 except for $G_a = 0.6\kappa$ and $P_d = 150\ \mu$W.

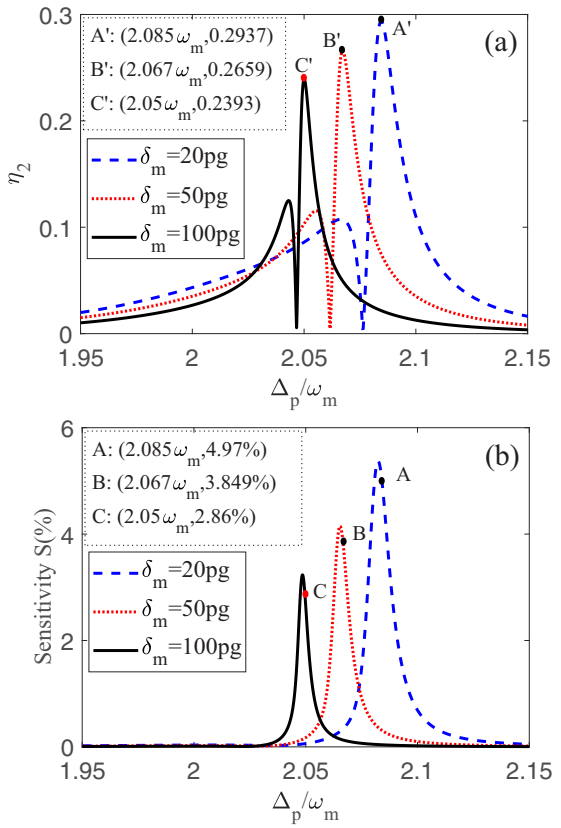

FIG. 7. (a) The efficiency η_2 of a second-order upper sideband and (b) the sensitivity S (in units of pg) of a mass sensor as a function of the probe-pulsed detuning Δ_p for different added mass δ_m. Other parameters are the same as in Fig. 2 except for $G_a = 0.6\kappa$ and $P_d = 150\ \mu$W.

extracting the maximum efficiency $\eta_2^{\max}$ and the corresponding optimum sensitivity $S_{\rm opt}$ in the same sideband spectrum, Fig. 8 shows the maximum efficiency $\eta_2^{\max}$ of a second-order upper sideband and the optimum sensitivity $S_{\rm opt}$ of a mass sensor varying with the added mass δ_m for different nonlinear gain G_a of DPA. When the added mass δ_m increases, the maximum efficiency $\eta_2^{\max}$ in Fig. 8(a) and the corresponding optimum sensitivity $S_{\rm opt}$ in Fig. 8(b) exhibit the overall decrease trends with an oscillatory variation. Direct comparison of Fig. 8(a) and Fig. 8(b) implies that the oscillatory variation of optimum sensitivity $S_{\rm opt}$ in Fig. 8(b) is more obvious than that in the maximum efficiency $\eta_2^{\max}$ of Fig. 8(a). In fact, this more obvious oscillation of the optimum sensitivity results from the position deviation between the maximum efficiency and the maximum sensitivity. From the viewpoint of application, the present optomechanical system, which creates synchronously the maximum efficiency of a second-order sideband and the optimum sensitivity, is suitable for the establishment of the high-sensitive mass sensor. More importantly, the oscillatory extent of maximum efficiency $\eta_2^{\max}$ depends essentially on the resolution of a mass sensor, because the overlap region of maximum efficiency induced by this efficiency oscillation cannot be distinguished in the present mass sensor based on the detection of the maximum efficiency variation. That is to say, if the same maximum efficiency of a second-order sideband is achieved in two optomechanical environments with two kinds of added mass, the mass difference between two kinds of added mass can be regarded as the minimum resolution of a mass sensor. For instance, in the case of the mass difference between two points D and D′ in the inset of Fig 8(a), the resolution of a mass sensor equates to 99.0 pg − 98.6 pg = 0.4 pg. From Fig. 8(a), it is easily checked that the smaller the added mass of membrane is, the higher the resolution of mass sensor becomes. Specially for the added mass within 100 pg, the minimum resolution of a sideband spectrum reaches 0.4 pg, which enables this mass sensor of an optomechanical system to achieve a high resolution at the pg level.

IV. NOISE ANALYSIS AND EXPERIMENTAL FEASIBILITY

Although system noise processes limit the performance of a high-precision mass sensor, there are various methods that can suppress these system noise processes and improve the detection sensitivity. As an example, we analyze how the photon shot noise is suppressed by using a quantum squeezed effect in the cavity optomechanical system. According to the perturbation method of $\mathcal{O}(t) = \mathcal{O}_0 + \delta\mathcal{O}(t)$ ($\mathcal{O} = a, X, P, Q$), $\delta\mathcal{O}(t)$ is the small fluctuation. By substituting perturbation forms into Eq. (2), we can obtain the linearized equation for the fluctuating operators:

$$\partial_t \delta a = -\left[\frac{\kappa}{2} + i(\Delta_c + GX_0)\right]\delta a - iGa\delta X + 2G_a\delta a^\dagger e^{-i\Delta_p t} + \sqrt{\eta_L\kappa}a_{in}, \tag{14}$$

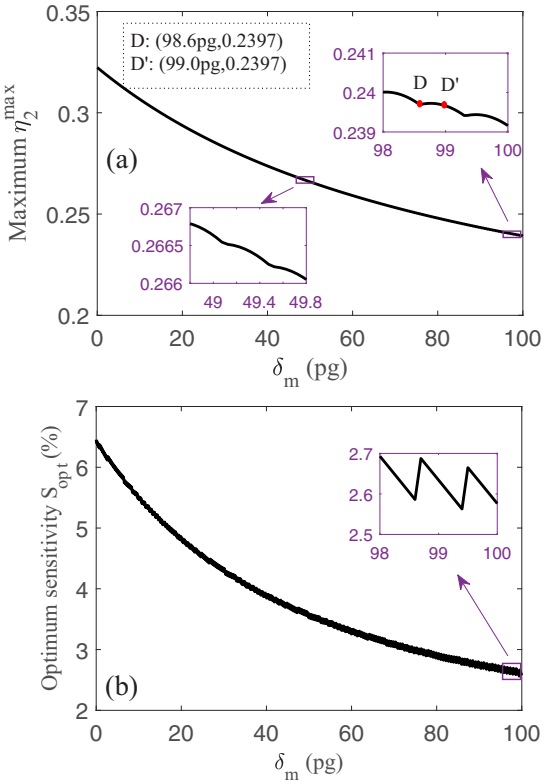

FIG. 8. (a) The maximum efficiency $\eta_2^{\max}$ of a second-order upper sideband and (b) the corresponding optimum sensitivity $S_{\rm opt}$ (in units of pg) of a mass sensor versus the added mass δ_m. Other parameters are the same as in Fig. 2 except for $G_a = 0.6\kappa$ and $P_d = 150\ \mu$W.

$$\partial_t \delta X = \frac{\delta Q}{m}, \tag{15}$$

$$\partial_t \delta P = -\left(2\hbar G|a_0|^2 + m\omega_m^2\right)\delta Q - 2\Gamma_m \delta P + F'_{th}, \tag{16}$$

$$\partial_t \delta Q = -\left(4\hbar G|a_0|^2 + 2m\omega_m^2\right)\delta X - \Gamma_m \delta Q + \frac{2\delta P}{m} - 4\hbar G(a_0 X_0 \delta a^\dagger + a_0^* X_0 \delta a). \tag{17}$$

Note that the incident fields support the intensity of the output field, while noise operators a_{in} and F'_{th} directly contribute to the fluctuation of the output field. Here, since we concentrate only on the quantum fluctuation induced by system photon shot noise, the incident fields are neglected in Eq. (14), and the thermomechanical noise F'_{th} needs to be excluded by setting $G = 0$. In this case, using the slowly varying fluctuation operators $\delta a = \delta\tilde{a}e^{-i\Delta_p t/2}$ and $a_{in} = \tilde{a}_{in}e^{-i\Delta_p t/2}$, Eq. (14) is rewritten as

$$\partial_t \delta\tilde{a} = -\left[\frac{\kappa}{2} + i\Delta_c - i\frac{\Delta_p}{2}\right]\delta\tilde{a} + 2G_a\delta\tilde{a}^\dagger + \sqrt{\eta_L\kappa}\tilde{a}_{in}. \tag{18}$$

Then, by considering a Fourier transform $f(t) = \frac{1}{2\pi}\int_{-\infty}^{+\infty} f(\omega)e^{-i\omega t}\,d\omega$ for operators $\delta\tilde{a}$, $\delta\tilde{a}^\dagger$ and noise source $\tilde{a}_{in}$, one can give the linearized fluctuation equation in the frequency domain

$$-i\omega\delta\tilde{a}(\omega) = -\left[\frac{\kappa}{2} + i\Delta_c - i\frac{\Delta_p}{2}\right]\delta\tilde{a}(\omega) + 2G_a\delta\tilde{a}^\dagger(\omega) + \sqrt{\eta_L\kappa}\tilde{a}_{in}(\omega). \tag{19}$$

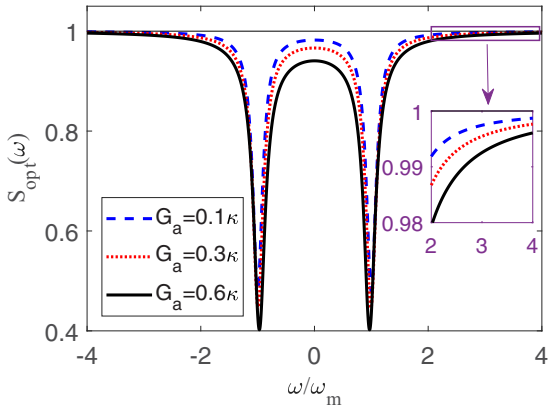

FIG. 9. The quadrature squeezing spectra for output light. Under the rotating frame of control field frequency ω_d, the central frequency $\omega = 0$ of the x axis corresponds to the position of ω_d. Other parameters are the same as in Fig. 2 except for $G = 0$, $\Delta_p = 2\omega_m$, and $P_d = 150\ \mu$W.

The solution for Eq. (19) is derived as

$$\delta\tilde{a}(\omega) = \frac{B_2\sqrt{\eta_L\kappa}\tilde{a}_{in}(\omega) + 2G_a\sqrt{\eta_L\kappa}\tilde{a}_{in}^\dagger(\omega)}{B_1B_2 - 4G_a^2}, \tag{20}$$

where $B_1 = \frac{\kappa}{2} + i\Delta_c - i\frac{\Delta_p}{2} - i\omega$ and $B_2 = \frac{\kappa}{2} - i\Delta_c + i\frac{\Delta_p}{2} - i\omega$. The output field of noisy fluctuation is related to the input noise via the standard input-output relation $\delta a_{\rm out}(\omega) = \sqrt{\eta_L\kappa}\delta\tilde{a}(\omega) - \tilde{a}_{in}(\omega)$. Note that the correlation of the noise operator in a frequency domain is expressed as $\langle\tilde{a}_{in}(\omega)\tilde{a}_{in}^\dagger(\omega')\rangle = 2\pi\delta(\omega + \omega')$. By simulating a practical approach as already used in Refs. [57,60,61], the optimum quadrature squeezing $S_{\rm opt}(\omega)$ can be obtained as

$$S_{\rm opt}(\omega) = C_{aa^\dagger}^{\rm out}(\omega) + C_{a^\dagger a}^{\rm out}(\omega) - 2\left|C_{aa}^{\rm out}(\omega)\right|, \tag{21}$$

with the parameter $C_{\xi\xi'}^{\rm out}(\omega) = \frac{1}{4\pi}\int d\omega' e^{i(\omega+\omega')t}\langle\delta\xi_{\rm out}(\omega)\delta\xi'_{\rm out}(\omega') + \delta\xi_{\rm out}(\omega')\delta\xi'_{\rm out}(\omega)\rangle$ (ξ and ξ' represent a or $a^\dagger$). The quadrature squeezing occurs in the condition of $S_{\rm opt}(\omega) < 1$, while $S_{\rm opt}(\omega) > 1$ represents nonsqueezing. It should be pointed out that $S_{\rm opt}(\omega) = 1$ corresponds to the spectra of fluctuation for a vacuum state or coherent light.

In the same cavity optomechanical environment of a nonlinear mass sensor, we plot the quadrature squeezing spectra in Fig. 9. Actually, the amount of squeezing in the quadrature squeezing spectra describes the level of photon shot noise. For example, $S_{\rm opt}(\omega) < 1$ means that the fluctuation of the output spectrum is below the standard quantum fluctuations (or the quantum shot noise limit). In this case, not only the above second-order sideband signal at the μW level but also gravitational waves can be efficiently measured [62]. In these squeezing spectra of Fig. 9, one finds that the amount of squeezing slightly increases with nonlinear gain G_a increasing. This result indicates that DPA plays an important role in reducing the level of shot noise. From the three squeezed spectra, we also find that the amount of squeezing at the frequency of the second-order sideband (i.e., $\omega \simeq 4\omega_m$) is below the quantum shot noise limit [i.e., $S_{\rm opt}(\omega) < 1$[. Consequently, the present cavity optomehcanical system assisted by DPA is competent for achieving the all-optical mass sensor.

In addition to photon shot noise mentioned above, how to manage the other noise processes in the present optomechanical system needs to be introduced. (1) This sophisticated optomechanical device, which is used to explore the boundary between quantum and classical physics, should be operated in the low-temperature environment, which can avoid some extrinsic and intrinsic thermal noises. (2) The membrane's Brownian motion, that is, the dominant mechanical noise, can be limited by laser precooling [6–8,22]. More specially, an ultralow membrane's effective temperature with 6.82 mK has been realized in the quadratically coupled optomechanical system, as described in Ref. [22]. In this case, the membrane' Brownian motion is essentially suppressed, so that the quantum jumps of the membrane can be observed. As a result, the present optomechanical system has a robust ability for resisting these noise processes.

Before coming to a conclusion, we give a concise description of the experimental feasibility of our proposed mass sensor. For the quadratically coupled optomechanical system, these achievements of the present proposal including the nonlinear second-order sideband, the detection for the added mass, and the membrane energy require a strong quadratic optomechanical coupling between the cavity field and the membrane's displacement. Fortunately, recent experiments have allowed the quadratic optomechanical coupling to increase several orders of magnitude beyond previous devices [22–24]. In these works, the special optomechanical systems are fabricated in a high-finesse Fabry-Pérot cavity with good mechanical properties (high Q; small m, spring constant k), in which a SiN membrane is mounted to the waist of the cavity field. This optomechanical device with high finesse has an experimental repeatability even when the membrane is precisely placed at a node or antinode of the cavity field [22]. In addition, the assisted DPA can be realized by integrating a strong second-order nonlinearity material of lithium niobate or aluminum nitride into an optomechanical cavity [63–65]. Based on the excellent second-order nonlinear property of lithium niobate and the present mature deposition technology, a stable, narrow-line tunable, low-threshold optical parametric oscillator was experimentally reported in a whispering gallery mode resonator [63]. This report opens the possibility to combine the nonlinearity crystalline materials with an optomechanical system. Moreover, the measured sample of a micro- and nanoscale particle, such as single biomolecules, viruses, and nanoparticles, can be safely placed on the dielectric membrane without the additional interaction [39,40,66]. We believe that this nonlinear all-optical mass sensor is feasible under the existing experimental techniques of an optomechanical cavity with microstructured materials.

V. CONCLUSION

In conclusion, we have performed a theoretical analysis for realizing a high-sensitive mass sensor in the quadratically coupled optomechanical system. In this membrane-in-the-middle optomechanical configuration, the DPA is embedded into the optomechanical cavity driven by a strong control field and a weak probe pulse. By employing the perturbation method, we derive explicitly analytical expressions for the efficiency of a second-order sideband and the sensitivity of a mass sensor beyond the conventional linearized approximation. Comparing with the other state-of-the-art ultrasmall mass sensor, like the single optical detection and the electrical measurement, our proposed nonlinear mass sensor has several advantages. First, with the aid of a DPA-induced nonlinear parametrical process, our results show that nonlinear gain of DPA allows us to enhance the efficiency of a second-order sideband and improve the sensitivity of a nonlinear mass sensor beyond what is achievable in the linearly coupled optomechanical system based on the detection of mechanical frequency shift. Second, in the process of nonlinear mass detection, a cavity optomechanical system assisted by DPA has a robust ability for resisting various noises. Third, due to the compact micron-scale optical structure, this cavity optomechanical device emerges as an excellent platform for realizing large-scale integration. Fourth, considering the readability of the membrane's energy eigenstate in the quadratically coupled optomechanical system, this nonlinear mass sensor can be used to provide an additional functionality for detecting the energy of a membrane. Finally, this nonlinear mass sensor based on monitoring the efficiency variation of a second-order sideband can reach a high resolution at the pg level. Consequently, these results illustrate the potential to utilize the nonlinear dynamics of the quadratically coupled optomechanical system for designing an all-optical nonlinear mass detector.

ACKNOWLEDGMENTS

The research is supported in part by the National Natural Science Foundation of China under Grants No. 61522501, 61475024, 61675004, 61705107, 61727817, 61775098, and 61720106015; in part by the National High Technology 863 Program of China with Grants No. 2015AA015501 and 2015AA015502; and in part by Beijing Young Talent with Grant No. 2016000026833ZK15, Fund of the State Key Laboratory of IPOC (BUPT). W.-X.Y. is supported in part by the National Natural Science Foundation of China under Grants No. 11374050 and 11774054, in part by the Natural Science Foundation of Jiangsu Province under Grant No. BK20161410, and the Qing Lan project of Jiangsu. J.F.W. is supported by the National Natural Science Foundation of China under Grant No. 11504175.

APPENDIX

If the operator $\hat{b}$ ($\hat{b}^\dagger$) is used to describe the quantization for the position and momentum operators of the membrane via a relationship of $\hat{b} = (\hat{b}^\dagger)^\dagger = \sqrt{m\omega_m/2\hbar}(\hat{x} + i\hat{p}/m\omega_m)$ in the quadratically coupled optomechanical system, we have motion equations of operators $\hat{b}$ and $\hat{b}^\dagger$ as

$$\partial_t \hat{b} = -\frac{i\hbar G\hat{a}^\dagger\hat{a}}{m\omega_m}(\hat{b}^\dagger + \hat{b}) - i\omega_m\hat{b} - \Gamma_m\hat{b} + \hat{b}_{in}, \quad \text{(A1)}$$

$$\partial_t \hat{b}^\dagger = \frac{i\hbar G\hat{a}^\dagger\hat{a}}{m\omega_m}(\hat{b} + \hat{b}^\dagger) + i\omega_m\hat{b}^\dagger - \Gamma_m\hat{b}^\dagger + \hat{b}^\dagger_{in}, \quad \text{(A2)}$$

where $\hat{b}_{in}$ ($\hat{b}^\dagger_{in}$) is the annihilation (creation) operator of thermal noise. To simplify the above differential equations (A1) and (A2), we assume $G = 0$. Then under a rotating frame at

the frequency of ω_m by employing $\hat{b} = b(t)e^{-i\omega_m t}$, the general solution of Eqs. (A1) and (A2) can be given as

$$b(t) = b(0)e^{-\Gamma_m t} + \int_0^t dt' e^{-\Gamma_m(t-t')} b_{in}(t'), \tag{A3}$$

$$b^\dagger(t) = b^\dagger(0)e^{-\Gamma_m t} + \int_0^t dt' e^{-\Gamma_m(t-t')} b_{in}^\dagger(t'). \tag{A4}$$

Comparing Eqs. (A1) and (A2) with Eq. (4), one can find $\hat{F}_{th} = -i\sqrt{\frac{m\hbar\omega_m}{2}}(\hat{b}_{in} - \hat{b}_{in}^\dagger)$. Based on the general solution in Eqs. (A3) and (A4) and the relationship $\hat{p} = -i\sqrt{\frac{m\hbar\omega_m}{2}}(\hat{b} - \hat{b}^\dagger)$, we also obtain

$$p(t) = p(0)e^{-\Gamma_m t} + \int_0^t dt' e^{-\Gamma_m(t-t')} F_{th}(t'). \tag{A5}$$

According to the Heisenberg-Langevin equation, the dynamical motion of square-momentum operator $\hat{P}$ can be expressed as

$$\partial_t \hat{P} = (\partial_t \hat{p})\hat{p} + \hat{p}(\partial_t \hat{p}) = -\left(m\omega_m^2 + 2\hbar G\hat{a}^\dagger\hat{a}\right)(\hat{x}\hat{p} + \hat{p}\hat{x}) - 2\Gamma_m\hat{p}^2 + \hat{F}'_{th}, \tag{A6}$$

where the noise operator $\hat{F}'_{th} = \hat{F}_{th}\hat{p} + \hat{p}\hat{F}_{th}$ originates from the derivation of the thermal mechanical operator $\hat{F}_{th}$.

Next, we turn to solve the expectation value of $\langle\hat{F}'_{th}(t)\rangle$. By using the general solution of Eq. (A5) and $\hat{F}_{th} = -i\sqrt{\frac{m\hbar\omega_m}{2}}(\hat{b}_{in} - \hat{b}_{in}^\dagger)$, we have

$$\begin{aligned}\langle\hat{F}'_{th}(t)\rangle &= \langle\hat{F}_{th}(t)\hat{p}(t)\rangle + \langle\hat{p}(t)\hat{F}_{th}(t)\rangle = 2p(0)\langle\hat{F}_{th}(t)\rangle e^{-\Gamma_m t} \\ &\quad + 2\int_0^t dt' e^{-\Gamma_m(t-t')}\langle\hat{F}_{th}(t)\hat{F}_{th}(t')\rangle \\ &= 2\Gamma_m(2n_{th}+1)\frac{m\hbar\omega_m}{2}.\end{aligned} \tag{A7}$$

In the above formula derivation, the noise correlation functions associated with the input fluctuations are given by $\langle\hat{b}_{in}(t), \hat{b}_{in}^\dagger(t')\rangle = 2\Gamma_m(n_{th}+1)\delta(t-t')$ and $\langle\hat{b}_{in}^\dagger(t), \hat{b}_{in}(t')\rangle = 2\Gamma_m n_{th}\delta(t-t')$ with the mean thermal phonon number n_{th}.

[1] M. Aspelmeyer, T. J. Kippenberg, and F. Marquardt, Cavity optomechanics, Rev. Mod. Phys. **86**, 1391 (2014).

[2] M. Bhattacharya, H. Uys, and P. Meystre, Optomechanical trapping and cooling of partially reflective mirrors, Phys. Rev. A **77**, 033819 (2008).

[3] A. Schliesser, O. Arcizet, R. Riviere, G. Anetsberger, and T. J. Kippenberg, Resolved-sideband cooling and position measurement of a micromechanical oscillator close to the Heisenberg uncertainty limit, Nat. Phys. **5**, 509 (2009).

[4] S. Weis, R. Rivière, S. Deléglise, E. Gavartin, O. Arcizet, A. Schliesser, and T. J. Kippenberg, Optomechanically induced transparency, Science **330**, 1520 (2010).

[5] A. H. Safavi-Naeini, T. P. Mayer Alegre, J. Chan, M. Eichenfield, M. Winger, Q. Lin, J. T. Hill, D. E. Chang, and O. Painter, Electromagnetically induced transparency and slow light with optomechanics, Nature (London) **472**, 69 (2011).

[6] C. H. Metzger and K. Karrai, Cavity cooling of a microlever, Nature (London) **432**, 1002 (2004).

[7] S. Gigan, H. R. Böhm, M. Paternostro, F. Blaser, G. Langer, J. B. Hertzberg, K. C. Schwab, D. Bäuerle, M. Aspelmeyer, and A. Zeilinger, Self-cooling of a micromirror by radiation pressure, Nature (London) **444**, 67 (2006).

[8] O. Arcizet, P.-F. Cohadon, T. Briant, M. Pinard, and A. Heidmann, Radiation-pressure cooling and optomechanical instability of a micromirror, Nature (London) **444**, 71 (2006).

[9] H. Xiong, L.-G. Si, A.-S. Zheng, X. Yang, and Y. Wu, Higher-order sidebands in optomechanically induced transparency, Phys. Rev. A **86**, 013815 (2012).

[10] H. Xiong, L.-G. Si, X.-Y. Lü, X. Yang, and Y. Wu, Carrier-envelope phase-dependent effect of high-order sideband generation in ultrafast driven optomechanical system, Opt. Lett. **38**, 353 (2013).

[11] H. Xiong, L.-G. Si, X.-Y. Lü, X. Yang, and Y. Wu, Nanosecond-pulse-controlled higher-order sideband comb in a GaAs optomechanical disk resonator in the non-perturbative regime, Ann. Phys. **349**, 43 (2014).

[12] H. Xiong, L.-G. Si, X.-Y. Lü, and Y. Wu, Optomechanically induced sum sideband generation, Opt. Express **24**, 5773 (2016).

[13] H. Xiong, Y.-W. Fan, X. Yang, and Y. Wu, Radiation pressure induced difference-sideband generation beyond linearized description, Appl. Phys. Lett. **109**, 061108 (2016).

[14] Z. X. Liu, H. Xiong, and Y. Wu, Generation and amplification of a high-order sideband induced by two-level atoms in a hybrid optomechanical system, Phys. Rev. A **97**, 013801 (2018).

[15] Y. Jiao, H. Lü, J. Qian, Y. Li, and H. Jing, Nonlinear optomechanics with gain and loss: Amplifying higher-order sideband and group delay, New J. Phys. **18**, 083034 (2016).

[16] X. Y. Lü, J. Q. Liao, L. Tian, and F. Nori, Steady-state mechanical squeezing in an optomechanical system via Duffing nonlinearity, Phys. Rev. A **91**, 013834 (2015).

[17] X. Y. Lü, Y. Wu, J. R. Johansson, H. Jing, J. Zhang, and F. Nori, Squeezed Optomechanics with Phase-Matched Amplification and Dissipation, Phys. Rev. Lett. **114**, 093602 (2015).

[18] J. Q. Liao and C. K. Law, Parametric generation of quadrature squeezing of mirrors in cavity optomechanics, Phys. Rev. A **83**, 033820 (2011).

[19] S. Liu, W.-X. Yang, Z. Zhu, T. Shui, and L. Li, Quadrature squeezing of a higher-order sideband spectrum in cavity optomechanics, Opt. Lett. **43**, 9 (2018).

[20] G. S. Agarwal and S. Huang, Strong mechanical squeezing and its detection, Phys. Rev. A **93**, 043844 (2016).

[21] T. P. Purdy, P. L. Yu, R. W. Peterson, N. S. Kampel, and C. A. Regal, Strong Optomechanical Squeezing of Light, Phys. Rev. X **3**, 031012 (2013).

[22] J. D. Thompson, B. M. Zwickl, A. M. Jayich, F. Marquardt, S. M. Girvin, and J. G. E. Harris, Strong dispersive coupling of a high-finesse cavity to a micromechanical membrane, Nature (London) **452**, 72 (2008).

[23] J. C. Sankey, C. Yang, B. M. Zwickl, A. M. Jayich, and J. G. E. Harris, Strong and tunable nonlinear optomechanical coupling in a low-loss system, Nat. Phys. **6**, 707 (2010).

[24] A. M. Jayich, J. C. Sankey, B. M. Zwickl, C. Yang, J. D. Thompson, S. M. Girvin, A. A. Clerk, F. Marquardt, and J. G. E. Harris, Dispersive optomechanics: A membrane inside a cavity, New J. Phys. **10**, 095008 (2008).

[25] H. Miao, S. Danilishin, T. Corbitt, and Y. Chen, Standard Quantum Limit for Probing Mechanical Energy Quantization, Phys. Rev. Lett. **103**, 100402 (2009).

[26] S. Huang and G. S. Agarwal, Electromagnetically induced transparency from two-phonon processes in quadratically coupled membranes, Phys. Rev. A **83**, 023823 (2011).

[27] M. Karuza, C. Biancofiore, M. Bawaj, C. Molinelli, M. Galassi, R. Natali, P. Tombesi, G. Di Giuseppe, and D. Vitali, Optomechanically induced transparency in a membrane-in-the-middle setup at room temperature, Phys. Rev. A **88**, 013804 (2013).

[28] L. G. Si, H. Xiong, M. S. Zubairy, and Y. Wu, Optomechanically induced opacity and amplification in a quadratically coupled optomechanical system, Phys. Rev. A **95**, 033803 (2017).

[29] S. Liu, W. X. Yang, T. Shui, Z. Zhu, and A. X. Chen, Tunable two-phonon higher-order sideband amplification in a quadratically coupled optomechanical system, Sci. Rep. **7**, 17637 (2017).

[30] X. Y. Lü, L. L. Zheng, G. L. Zhu, and Y. Wu, Single-Photon-Triggered Quantum Phase Transition, Phys. Rev. Appl. **9**, 064006 (2018).

[31] A. Nunnenkamp, K. Børkje, J. G. E. Harris, and S. M. Girvin, Cooling and squeezing via quadratic optomechanical coupling, Phys. Rev. A **82**, 021806(R) (2010).

[32] M. Abdi, P. Degenfeld-Schonburg, M. Sameti, C. Navarrete-Benlloch, and M. J. Hartmann, Dissipative Optomechanical Preparation of Macroscopic Quantum Superposition States, Phys. Rev. Lett. **116**, 233604 (2016).

[33] M. R. Vanner, Selective Linear or Quadratic Optomechanical Coupling Via Measurement, Phys. Rev. X **1**, 021011 (2011).

[34] H. Tan, F. Bariani, G. Li, and P. Meystre, Generation of macroscopic quantum superpositions of optomechanical oscillators by dissipation, Phys. Rev. A **88**, 023817 (2013).

[35] J.-Q. Zhang, Y. Li, M. Feng, and Y. Xu, Precision measurement of electrical charge with optomechanically induced transparency, Phys. Rev. A **86**, 053806 (2012).

[36] H. Xiong, L. G. Si, and Y. Wu, Precision measurement of electrical charges in an optomechanical system beyond linearized dynamics, Appl. Phys. Lett. **110**, 171102 (2017).

[37] H. Xiong, Z. X. Liu, and Y. Wu, Highly sensitive optical sensor for precision measurement of electrical charges, Opt. Lett. **42**, 3630 (2017).

[38] C. Kong, H. Xiong, and Y. Wu, Coulomb-interaction-dependent effect of high-order sideband generation in an optomechanical system, Phys. Rev. A **95**, 033820 (2017).

[39] F. Liu and M. Hossein-Zadeh, Mass sensing with optomechanical oscillation, IEEE Sensors **13**, 146 (2013).

[40] F. Liu, S. Alaie, Z. C. Leseman, and M. Hossein-Zadeh, Sub-pg mass sensing and measurement with an optomechanical oscillator, Opt. Express **21**, 19555 (2013).

[41] J. J. Li and K. D. Zhu, Nonlinear optical mass sensor with an optomechanical microresonator, Appl. Phys. Lett. **101**, 141905 (2012).

[42] J. J. Li and K. D. Zhu, All-optical mass sensing with coupled mechanical resonator systems, Phys. Rep. **525**, 223 (2013).

[43] J. Chaste, A. Eichler, J. Moser, G. Ceballos, R. Rurali, and A. Bachtold, A nanomechanical mass sensor with yoctogram resolution, Nat. Nanotechnol. **7**, 301 (2012).

[44] Q. Lin, B. He, and M. Xiao, Mass sensing by detecting the quadrature of a coupled light field, Phys. Rev. A **96**, 043812 (2017).

[45] E. Buks and B. Yurke, Mass detection with a nonlinear nanomechanical resonator, Phys. Rev. E **74**, 046619 (2006).

[46] M. D. Dai, K. Eom, and C. W. Kim, Nanomechanical mass detection using nonlinear oscillations, Appl. Phys. Lett. **95**, 203104 (2009).

[47] Z. Yie, M. A. Zielke, C. B. Burgner, and K. L. Turner, Comparison of parametric and linear mass detection in the presence of detection noise, J. Micromech. Microeng. **21**, 025027 (2011).

[48] X. Liu, Y. Li, and H. Jing, Casimir switch: Steering optical transparency with vacuum forces, Sci. Rep. **6**, 27102 (2016).

[49] S. Huang and G. S. Agarwal, Robust force sensing for a free particle in a dissipative optomechanical system with a parametric amplifier, Phys. Rev. A **95**, 023844 (2017).

[50] F. Vollmer and S. Arnold, Whispering-gallery-mode biosensing: Label-free detection down to single molecules, Nat. Methods **5**, 591 (2008).

[51] K. L. Ekinci, Y. T. Yang, and M. L. Roukes, Ultimate limits to inertial mass sensing based upon nanoelectromechanical systems, J. Appl. Phys. **95**, 2682 (2004).

[52] L. Shao, X.-F. Jiang, X.-C. Yu, B.-B. Li, W. R. Clements, F. Vollmer, W. Wang, Y.-F. Xiao, and Q. Gong, Detection of single nanoparticles and lentiviruses using microcavity resonance broadening, Adv. Mater. **25**, 5616 (2013).

[53] M. O. Scully and M. S. Zubairy, *Quantum Optics* (Cambridge University Press, Cambridge, 1997).

[54] S. Shahidani, M. H. Naderi, and M. Soltanolkotabi, Control and manipulation of electromagnetically induced transparency in a nonlinear optomechanical system with two movable mirrors, Phys. Rev. A **88**, 053813 (2013).

[55] S. Huang and G. S. Agarwal, Enhancement of cavity cooling of a micromechanical mirror using parametric interactions, Phys. Rev. A **79**, 013821 (2009).

[56] S. M. Spillane, T. J. Kippenberg, O. J. Painter, and K. J. Vahala, Ideality in a Fiber-Taper-Coupled Microresonator System for Application to Cavity Quantum Electrodynamics, Phys. Rev. Lett. **91**, 043902 (2003).

[57] C. W. Gardiner and P. Zoller, *Quantum Noise*, 3rd ed. (Springer-Verlag, Berlin, 2004).

[58] W. X. Yang, A. X. Chen, X. T. Xie, and L. Ni, Enhanced generation of higher-order sidebands in a single-quantum-dotcavity system coupled to a $\mathcal{PT}$-symmetric double cavity, Phys. Rev. A **96**, 013802 (2017).

[59] A. Butsch, J. R. Koehler, R. E. Noskov, and P. St. J. Russell, CW-pumped single-pass frequency comb generation by resonant optomechanical nonlinearity in dual-nanoweb fiber, Optica **1**, 158 (2014).

[60] S. Mancini and P. Tombesi, Quantum noise reduction by radiation pressure, Phys. Rev. A **49**, 4055 (1994).

[61] U. S. Sainadh and M. A. Kumar, Effects of linear and quadratic dispersive couplings on optical squeezing in an optomechanical system, Phys. Rev. A **92**, 033824 (2015).

[62] The LIGO Scientific Collaboration, A gravitational wave observatory operating beyond the quantum shot-noise limit, Nat. Phys. **7**, 962 (2011).

[63] J. U. Fürst, D. V. Strekalov, D. Elser, A. Aiello, U. L. Andersen, C. Marquardt, and G. Leuchs, Low-Threshold Optical Parametric Oscillations in a Whispering Gallery Mode Resonator, Phys. Rev. Lett. **105**, 263904 (2010).

[64] A. Guarino, G. Poberaj, D. Rezzonico, R. Degl'Innocenti, and P. Günter, Electro-optically tunable microring resonators in lithium niobate, Nat. Photon. **1**, 407 (2007).

[65] C. Xiong, W. H. Pernice, X. Sun, C. Schuck, K. Y. Fong, and H. X. Tang, Aluminum nitride as a new material for chip-scale optomechanics and nonlinear optics, New J. Phys. **14**, 095014 (2012).

[66] J. L. Arlett, E. B. Myers, and M. L. Roukes, Comparative advantages of mechanical biosensors, Nat. Nanotech. **6**, 203 (2011).